Ribosome biogenesis is a downstream effector of the oncogenic U2AF1-S34F mutation

Abdalla Akef[1], Steven D. Cappell[2] and Daniel R. Larson[1,3,*]

[1]Laboratory of Receptor Biology and Gene Expression, National Cancer Institute, NIH, Bethesda, MD, 20892, USA

[2]Laboratory of Cancer Biology and Genetics, National Cancer Institute, NIH, Bethesda, MD, 20892, USA

[3]Lead Contact

Correspondence: dan.larson@nih.gov (D.R.L)

Running title: Ribosome biogenesis is downstream of U2AF1-S34F mutant

Abstract

U2 Small Nuclear RNA Auxiliary Factor 1 (U2AF1) forms a heterodimeric complex with U2AF2 that is responsible for 3' splice site selection. U2AF1 mutations have been identified in Myelodysplastic Syndrome (MDS) and Lung Adenocarcinoma (LUAD) patients, the most common of which is a single missense substitution of serine-34 to phenylalanine (S34F). However, there is no clear set of splicing alterations which explain the tumorigenic role of the U2AF1-S34F mutation. Previously, we reported that the U2AF1-S34F mutation enhances the translation of U2AF1 target mRNAs which are enriched for ribosome biogenesis factors. Among the translationally upregulated targets of U2AF1-S34F are Nucleophosmin1 (NPM1) and Importin 7 (IPO7). Here we report that U2AF1-S34F promotes global mRNA translation. Depletion of NPM1 or IPO7 impairs the viability of wt/S34F cells, and the cells have a lower proliferative capacity and suffer rRNA processing defects. Our results indicate an unanticipated connection between U2AF1, NPM1, ribosome biogenesis.

Introduction

U2AF1 (also known as U2AF35) forms a heterodimeric complex with U2AF2 (U2AF65) that is responsible for 3' splice site selection (Merendino et al., 1999). Several U2AF1 mutations have been identified in Myelodysplastic Syndrome (MDS) and Lung Adenocarcinoma (LUAD) patients (Brooks et al., 2014), the most common of which is a single missense substitution of serine-34 to phenylalanine (S34F). The mutation is heterozygous, occurs early in disease progression, and is a hotspot mutation in the RNA binding domain of the protein, strongly suggesting a gain of function, oncogenic mutation. While several groups have examined alternative splicing alterations that are mediated by the S34F mutation (Brooks et al., 2014; Fei et al., 2016; Yoshida et al., 2011), there is no clear set of splicing events that can explain the tumorigenic role of the S34F mutation. Previously, we reported that U2AF1, in complex with U2AF2, plays a non-canonical role in translation regulation through direct interactions with target RNA in the cytosol (Palangat et al., 2019). Using RNA immunoprecipitation (RIP) and polysome profiling, we found that the S34F mutation resulted in loss of binding and a concomitant increase in the translation of these target mRNAs. These mRNA targets were enriched for components of the mRNA translation and ribosome biogenesis machinery (Palangat et al., 2019). However, it is unknown how ribosome biogenesis and translational misregulation play a role in the physiology of U2AF1 mutations and contribute to leukemogenesis.

Among the top translationally upregulated targets of U2AF1-S34F are Nucleophosmin1 (NPM1) and Importin 7 (IPO7), which play functional roles in ribosome biogenesis. Ribosome biogenesis is initiated when RNA polymerase I transcribes ribosomal DNA (rDNA) into the 47S pre-ribosomal RNA (rRNA) transcript that encompasses the 18S, 5.8S and the 28S flanked by 2 external (5' external transcribed spacer (5' ETS) and 3' ETS) and interspersed by 2 internal spacers (internal transcribed spacer 1 (ITS1) and ITS2). The 18S rRNA and small subunit ribosomal proteins constitute the pre-40S ribosomal subunit. The 28S, 5.8S, and 5S (produced by RNA polymerase III) along with the large subunit ribosomal proteins constitute the pre-60S subunit. NPM1 (also known as B23) is a nucleic acid binding

protein responsible for the processing of the ITS2 (Herrera et al., 1995; Savkur and Olson, 1998), nucleocytoplasmic transport of both the 28S and 18S rRNA (Maggi et al., 2008), and localization of the ITS2-cleaving endonuclease LAS1L to the nucleolus (Castle et al., 2012). IPO7 is responsible for the import of the large ribosomal subunit proteins RPL5 and RPL11 to the nucleus (Golomb et al., 2012). Despite the involvement of NPM1 and IPO7 in a crucial process such as ribosome biogenesis, fibroblasts derived from an *NPM1*$^{-/-}$ mouse could survive in culture with modest defects (Grisendi et al., 2005). Moreover, the expression of a dominant-negative NPM1 mutant did not cause noticeable defects in the steady state levels of the 28S and 18S rRNA (Maggi et al., 2008). IPO7 silencing by RNA interference (RNAi) was not reported to cause cell death (Golomb et al., 2012). These findings suggest that NPM1 and IPO7 are not required for cell viability.

NPM1 is mutated in a fifth of all AML cases and the AML-linked mutations cause the mislocalization of NPM1 to the cytoplasm (Falini et al., 2005) potentially leading to an imbalance of nucleolar and cytoplasmic functions. For example, the cytoplasmic accumulation of NPM1 has been shown to promote cell proliferation and increase HOX gene expression (Brunetti et al., 2018). In addition, NPM1 downregulates the activity of p53 by sequestering ARF (also known as p14) in the nucleolus and preventing the ARF-MDM2 interaction (Korgaonkar et al., 2005; Itahana et al., 2003; Bertwistle et al., 2004). This sequestration causes MDM2-mediated downregulation of p53. Strikingly, NPM1 mutations rarely occur outside of myeloid malignancies (i.e., MDS and AML), suggesting that NPM1 plays a unique role in the differentiation and/or growth of myeloid cells. However, the role of NPM1 in promoting myeloid malignancies remains incompletely understood. Despite the pervasiveness of splicing factor and NPM1 mutations in myeloid disease, there is no reported functional connection between these factors.

Here, we establish a direct link between two major drivers of myeloid disease – U2AF1 and NPM1. We find that cells with a heterozygous U2AF1-S34F mutation are dependent on NPM1 for cell-cycle progression. Depletion of NPM1 impaired the viability of the S34F-harboring cells but not wt/wt

cells as did the depletion of a second ribosome biogenesis factor, Importin 7 (IPO7) which is also a direct U2AF1 target in the cytoplasm. WT/S34F cells lacking NPM1 or IPO7 had a lower proliferative capacity and accumulated in S phase of the cell cycle and demonstrated rRNA processing defects. Our results demonstrate that NPM1 and IPO7 are downstream effectors of the translation changes mediated by the U2AF1-S34F mutation. Moreover, this viability defect explains why U2AF1 and NPM1 mutations are mutually exclusive in cancer patients. These data indicate an unanticipated functional connection between a splicing factor mutation and the ribosome biogenesis machinery.

Results and Discussion

The S34F mutation upregulates global translation

To dissect the molecular mechanisms perturbed by the U2AF1-S34F mutation, we employed three human bronchial epithelial cell lines (HBEC) (Ramirez et al., 2004) that were generated by gene-editing: (1) biallelic WT U2AF1 (herein referred to as wt/wt), (2) wt/U2AF1-S34F heterozygous (wt/S34F), and (3) a frameshift of the U2AF1-S34F allele (wt/S34F-) as previously described (Fei et al., 2016; Palangat et al., 2019). Using RNA immunoprecipitation followed by sequencing (RIP-seq), we reported that U2AF1 binds mRNA in the cytoplasm enriched for functional categories that include translation initiation and protein biosynthesis. By systematically analyzing polysome profiling data from wt/wt, wt/S34F and wt/S34F- cells (previously published in Palangat et al., 2019), we sought to determine whether the S34F mutation altered the translational regulation of ribosome biogenesis and translation factors. This analysis is based on a weighted estimator of translation efficiency as determined by RNA abundance in the polysome profile. We found that the S34F mutation specifically upregulated a large fraction of ribosome biogenesis and mRNA translation factors (Fig 1A). We confirmed the upregulation of NPM1 translation in wt/S34F cells using a dual luciferase reporter. The first exon of *NPM1* was fused upstream to Renilla luciferase. To normalize for differences in cell number and copy number, the reporter also included a Firefly luciferase downstream of an Internal Ribosome Entry Site (IRES) sequence

derived from the Cricket Paralysis Virus (CrPV) (Coller and Parker, 2005; Fernández et al., 2014) (Fig. 1B). The wt/S34F cells had an 8-fold higher Renilla to Firefly luciferase activity than wt/wt or wt/S34F- cells (Fig. 1C) further confirming the upregulation of NPM1 in cells harboring the U2AF1-S34F mutation and additionally indicating that the 5' end of the mRNA is sufficient for increased translation.

To examine the consequence of upregulation of the translation machinery, we compared global mRNA translation rates between the wt/wt and the wt/S34F cells using the fluorescent noncanonical amino acid tagging (FUNCAT) as previously described (Tom Dieck et al., 2012). Cells were pulsed with the methionine analog azido-homoalanine (AHA) for 1 hour. Subsequently, cells were fixed, permeabilized and the AHA-containing nascent polypeptides were labelled for microscopy using click chemistry. First, we confirmed that puromycin treatment abolished the AHA fluorescence signal (Fig. 1D). Next, we found that the S34F mutation caused an upregulation in global translation (Fig 1E, quantification in Fig.1F). Comparing fluorescence intensity at the single cell level indicated that the elevated level of global translation in the wt/S34F cells was representative of the whole cell population rather than a few outlier cells (Fig. 1G). Taken together, we conclude the wt/S34F cells have elevated levels of translation factors and the ribosome machinery along with an increase in global mRNA translation.

Wt/S34F cells require NPM1 and IPO7 for survival in a p53 independent manner

Among the top U2AF1 targets are NPM1 and IPO7, two factors which play important roles in ribosome biogenesis (Maggi et al., 2008; Golomb et al., 2012; Castle et al., 2012; Savkur and Olson, 1998). We sought to examine whether increased NPM1 translation was a downstream mediator of the pro-tumorigenic phenotype of the U2AF1-S34F mutation. NPM1 was depleted by RNAi in wt/wt, wt/S34F and wt/S34F- cells (Fig 2A). We noticed a marked decrease in the viability of the wt/S34F cells upon NPM1 depletion (Fig. 2B) concomitant with a decrease in metabolic activity (Fig 2C). No defects were observed for the wt/wt or wt/S34F- cells (Fig. 2B-C). IPO7 depletion also specifically impaired the

survival of wt/S34F (Fig. 2B, D-E). We generated cell lines that express an RNAi-resistant NPM1 construct (NPM1^{r}-2A-GFP) using lentiviral-mediated integration. A slower mobility band was detected for NPM1^{r}-2A-GFP that was unaffected by NPM1 siRNA treatment (Fig. 2F). The viability of the wt/S34F cells that express NPM1^{r}-2A-GFP was partially restored (Fig. 2G). The partial rescue is likely due to the low expression levels of NPM1^{r}-2A-GFP in comparison to endogenous NPM1 levels (Fig. 2F).

Since NPM1 sequesters ARF in the nucleolus leading to an MDM2-mediated downregulation of p53 (Korgaonkar et al., 2005; den Besten et al., 2005; Mariano et al., 2006), we investigated whether the viability defect of the wt/S34F cells depleted of NPM1 was dependent on p53 activity. First, we compared p53 levels between wt/wt and wt/S34F cells depleted of NPM1. NPM1 depletion caused the upregulation of p53 in both the wt/wt and wt/S34F cells to a comparable extent (Fig. 3A). Moreover, the synergistic depletion of NPM1 and p53 did not rescue the viability defect of the wt/S34F cells caused by the absence of NPM1 (Fig 3B-C). Next, we sought to assess if increasing p53 levels in an NPM1-independent mechanism would specifically impair the viability of the wt/S34F cells. p53 levels were induced by treating cells with 10µM Nutlin3A (Tovar et al., 2006) (Fig. 3D). p53 activation by increasing Nutlin3A concentration impaired the viability of wt/wt, wt/S34F and wt/S34F- cells to a similar extent (Fig. 3E, quantification in Fig. 3F). Thus, we conclude that the depletion of NPM1 impairs the viability of the wt/S34F cells through a p53-independent pathway.

Wt/S34F cells depleted of NPM1 suffer cell cycle progression defects

The viability defect observed in wt/S34F cells lacking NPM1 can be explained by either an activation of apoptotic pathways or a defect in cell cycle progression. To distinguish between these possibilities, we first examined cellular viability over the time course of the knock-down experiment. First, wt/wt cells transfected with control siRNA had comparable growth with wt/wt cells depleted of either NPM1 or IPO7. In contrast, wt/S34F cells depleted of NPM1 or IPO7 had a drastically lower viability than wt/S34F cells treated with control siRNA (Fig. 4A), consistent with our earlier observations

(Fig. 2B). Importantly, we observed a monotonic increase in the metabolic activity of the wt/S34F cells depleted of NPM1 or IPO7 over the time period of the measurement which is more consistent with slowed growth rates and not an induction of apoptotic pathways. We further confirmed the lack of apoptosis by comparing Active Caspase-3 levels. We chose Caspase-3 since it is one of the late apoptotic factors and thus is activated by both the extrinsic and intrinsic apoptotic pathways. We did not observe a difference in active Caspase-3 levels between wt/wt and wt/S34F cells treated with either control or NPM1 siRNA suggesting that apoptosis is not the cause of decreased viability in the wt/S34F cells lacking NPM1 activity (Fig. 4B, Supplementary Fig. 1A). In contrast, ActinomycinD treatment (5ug/mL) caused a robust upregulation in Caspase-3 levels.

Next, we examined whether wt/S34F cells depleted of NPM1 had cell cycle progression defects. Cells were treated with 5-ethynyl-2´-deoxyuridine (EdU) for 10 minutes to label the S phase population (Salic and Mitchison, 2008). The G1 and G2 cell populations were identified by quantifying the DNA fluorescence intensity using Hoechst (Fig. 4C, Supplementary Fig. 1B). The depletion of NPM1 in wt/wt cells did not have a measurable effect on cell cycle progression. In contrast, the absence of NPM1 from the wt/S34F cells led to an increase in the fraction of S phase cells and a concomitant decrease in the G1 population (Fig. 4C). These results indicate that wt/S34F cells depleted of NPM1 take a longer time to complete S phase. Expression of NPM1^{r}-2A-GFP in wt/S34F when NPM1 is silenced restored the S phase population to control siRNA levels (Fig. 4C). We also observed elevated levels of the S phase population in wt/S34F cells when IPO7 was silenced (Fig. 4D, Supplementary Fig. 1C). We further confirmed the accumulation of cells in S phase by examining the levels of Cyclin A2 (CCNA2), which is upregulated in S, G2 and early M phase. Indeed, Cyclin A2 levels were specifically upregulated in wt/S34F cells depleted of NPM1 (Fig. 4E) or IPO7 (Fig. 4F). Silencing NPM1 or IPO7 expression in wt/wt cells did not have a detectable effect on Cyclin A2 levels. In summary, the absence of NPM1 or IPO7 caused the accumulation of wt/S34F cells in S phase leading to slower growth and a proliferative disadvantage.

Processing of the 28S rRNA precursors is impaired in wt/S34F cells depleted of NPM1 or IPO7.

NPM1 has been previously shown to bind the 28S rRNA (Huang et al., 2005) and regulate the processing of the 28S rRNA by promoting the localization of the endoribonuclease LAS1L to the nucleolus (Castle et al., 2012). Moreover, IPO7 coordinates the nuclear import of RPL5 and RPL11, two components of the large ribosomal subunit. Therefore, we reasoned that silencing NPM1 or IPO7 might cause a specific impairment in the processing of the 28S rRNA precursors. We examined the levels of the 28S rRNA precursors by employing Northern blot using a probe complementary in sequence to the ITS2 (Donati et al., 2013). Silencing NPM1 or IPO7 in wt/wt cells did not cause a change in the levels of the ITS2-containing precursors. In contrast, the levels of the ITS2 precursors in wt/S34F cells decreased after NPM1 or IPO7 were depleted (Fig. 5A-B). The levels of *GAPDH* mRNA demonstrate equal loading across samples. However, the decrease in the ITS2 precursors did not cause a noticeable change in mature 28S and 18S rRNA levels likely due to their long half-life ranging from three to seven days (Halle et al., 1997; Gillery et al., 1995).

U2AF1 and NPM1 simultaneous mutations are significantly underrepresented in cancer patients.

Since the S34F cells require NPM1 for their viability, we hypothesized that the S34F mutation should not co-occur in cancer patients with NPM1 loss of function (LOF) mutations. Both *U2AF1* and *NPM1* are frequently mutated in patients with malignancies of the myeloid lineage. According to the cBioPortal database, *U2AF1* mutations occur in 5% and *NPM1* is mutated in 22% of all myeloid malignancy patients. Despite the high frequency of these mutations, we found that *U2AF1* and *NPM1* mutations co-occurred at a probability lower than that expected by chance (Fig. 5C), likely due to the deleterious viability defect caused by abolishing NPM1 function in cells harboring U2AF1 mutations. This analysis recapitulated other previously observed mutual dependencies. For example, *SRSF2* and *IDH2* are more likely to co-occur (Yoshimi et al., 2019). Notably, *NPM1* mutations were mutually exclusive with *U2AF1* mutations but not with other commonly mutated splicing factors such as *SF3B1*, *SRSF2* and *ZRSR2*.

In conclusion, our results demonstrate that the U2AF1-S34F mutation upregulates components of the translation and ribosome biogenesis machineries through changes in translation efficiency. The absence of NPM1 and IPO7 impairs the ability of the wt/S34F cells to proliferate due to an impairment in the cells' ability to progress through the S phase.

Although U2AF1 mutations have been implicated as driver mutations in lung cancer and acute myeloid leukemia, the role of these mutations in disease progression has remained elusive. Here, we demonstrate an unanticipated functional connection between U2AF1 and ribosome biogenesis. We show that the U2AF1-S34F mutation causes an increase in global translation at the single cell level. Furthermore, wt/S34F cells require ribosome biogenesis factors such as NPM1 and IPO7 to proliferate. In the absence of NPM1 and IPO7, the proliferative capacity of cells harboring the S34F mutation decreases. Importantly, the viability defect is independent of p53 since p53 is induced in both wt/wt and wt/S34F cells to a comparable level upon NPM1 depletion. This cell cycle defect is likely linked to a reduction in the production of the 28S rRNA precursors. The dependence of the S34F cells on NPM1 is further demonstrated by the fact that *U2AF1* and *NPM1* mutations are unlikely to co-occur in the same patient despite the fact that both *U2AF1* and *NPM1* are commonly mutated in myeloid malignancy.

While NPM1 has been reported to regulate p53 activity either directly (Colombo et al., 2002) or through ARF (Korgaonkar et al., 2005; Itahana et al., 2003; Bertwistle et al., 2004), several lines of evidence argue against a role for p53 in the viability defect of S34F cells depleted of NPM1. First, abrogating NPM1 expression causes comparable levels of p53 induction in both the wt/wt and wt/S34F cells (Fig. 3A). Second, co-depletion of NPM1 and p53 did not rescue the viability defect observed in single NPM1 depletion (Fig. 3B-C). Third, p53 activation by 20uM Nutlin3A caused a comparable impairment of the viability of wt/wt and wt/S34F cells (Fig. 3D-F).

Why are ribosome biogenesis factors specifically required for the viability and proliferation of wt/S34F cells but not wt/wt U2AF1 cells? We note that these experiments were performed in human

bronchial epithelial cells, which are an immortalized but non-transformed cell line (Ramirez et al., 2004). This system might better recapitulate splicing factor mutations, which usually occur early in disease progression (Abelson et al., 2018). In tissue, cells must strike a balance between proliferation, differentiation, and self-renewal, for example as demonstrated in hematopoiesis (Khajuria et al., 2018). This balance is altered in MDS, and hematopoietic stem cells derived from MDS patients have elevated mRNA translation levels (Stevens et al., 2018). Our isogenic cell culture system recapitulates this finding with only a single nucleotide change in the *U2AF1* gene. Moreover, we speculate that ribosome biogenesis factors such as NPM1 or IPO7 which are not required for cell viability under basal growth levels (Grisendi et al., 2005; Golomb et al., 2012) become crucial when mRNA translation levels are elevated due to the U2AF1-S34F mutation. The absence of NPM1 or IPO7 impairs the production of the 47S pre-rRNA precursor in wt/S34F cells and this slows cell proliferation and causes their accumulation in S phase. Indeed, NPM1 has been shown to localize to centrosomes and regulate their duplication suggesting potential links between ribosome biogenesis and cell division factors (Okuda et al., 2000; Grisendi et al., 2005). Moreover, mTOR, another growth-promoting signaling pathway, has been shown to upregulate NPM1 expression (Pelletier et al., 2007). It should be also noted that abrogating the expression of the small ribosome subunit protein, RPS6 impairs cell division (Volarevic et al., 2000). In sum, this study uncovered a novel dependence of cancer-associated U2AF1 mutations on ribosome biogenesis to maintain a highly proliferative state.

Materials and Methods

Plasmids and cells lines

The plasmid expressing the NPM1^{r}-2A-GFP reporter was generated by fusing the cDNA of NPM1 amplified from HBEC cDNA library upstream of 2A-GFP synthetic construct (IDT). This was subsequently inserted into a lentiviral transfer plasmid that has the Ubiquitin C promoter. The NPM1 luciferase reporter was generated by fusing 2 synthetic constructs (IDT) into the Ubiquitin C lentiviral

transfer plasmid. The first construct was composed of human NPM1 exon 1 sequence fused to Renilla luciferase. The second construct composed of CrPV IRES fused to firefly luciferase (Coller and Parker, 2005). The lentiviral plasmids were packaged into lentiviral particles using HEK293T cells. Viruses were collected from the supernatant and transduced into HBEC using 8ug/mL polybrene. HBEC lines were cultured in keratinocyte serum-free medium supplemented with bovine pituitary extract and epidermal growth factor (Invitrogen). Wt/wt, wt/S34F and wt/S34F- HBEC cells were previously reported (Fei et al., 2016). For translation inhibition experiments, cells were incubated with puromycin (100ug/mL) for 30 minutes prior to AHA treatment. Nutlin3A treatment was for 36 hours at the indicated doses. For Caspase-3 experiments, cells were treated with Actinomcycin D (5ug/mL) for 12 hours. For pladienolide B experiments, cells were treated for 2 days with the indicated doses. For siRNA experiments, cells were treated 25pmol smartpool siRNA (Dharmacon) and Lipofectamine RNAiMax transfection reagent (Thermo). Knock-down efficiency was assessed after 6 days by western blotting. The following siRNA pools were used: NPM1 (M-015737-01-0005), IPO7 (L-012255-00-0005), TP53 (L-003329-00-0005), RBM10 (E-009065-00-0005).

Polysome profile analysis

The following steps are used to compute changes in translation efficiency from polysome sequencing profiles measured in Palangat et al., 2019:

1) For each sample (wt/wt, wt/s34f, wt/s34f-), 12 fractions were collected from the sucrose gradient, and the bottom/heaviest 10 fractions were sequenced.

2) Fractions 10-12 were pooled to increase coverage, resulting in 8 fractions in the final analysis. Fraction 5 and 6 correspond to the monosome fractions.

3) Reads mapping to particular message are normalized by the total reads in that sample and multiplied by $1x10^6$, generating counts per million (CPM) for each transcript in each fraction.

4) The CPM in each fraction constitutes the polysome profile (poly(x), where ‘x’ designates the sucrose fraction) which is now normalized for read depth across fractions/samples.

5) This profile can be further normalized by a weighting function which accounts for the non-linear relationship between sedimentation coefficient, position in the sucrose gradient, and molecular mass: $S \sim x^{3/2}$, where *S* is the sedimentation coefficient in Svedrup (Marks, 2001). Here, we use the following weights for each fraction after pooling: *w*=[0.6, 1.0, 1.6, 2.2, 2.9, 3.7, 4.5, 19.0].

6) The final numeric value, reflecting translation efficiency, is $\sum w_i \mathrm{poly}(x_i)$. This number, generated for each transcript in each of the three cell lines, is the basis for clustering in Fig. 1A. Hierarchial clustering was done using ClustVis (Metsalu and Vilo, 2015).

Luciferase assay

Luciferase plasmids were introduced by lentiviral transduction. Equal number of cells were plated in a 96 well dish. After 24 hours, cells were treated with the Dual-Luciferase Reporter Assay System as per manufacturer's instructions (Promega). Luciferase activity was measured by Victor plate reader (Perkin Elmer).

AHA metabolic labeling

Global translation was assessed by AHA pulse labeling as previously described (Tom Dieck et al., 2012) with the following modification. Cells were plated on coverslips (VWR). After 24 hours, cells were pulsed with AHA for 1 hour. Cells were then fixed in 4% paraformaldehyde in PBS, permeabilized in 0.1% TritonX in PBS and blocked in blocking reagent that contains 2% BSA and 5% donkey serum in PBS for 3 hours. Cells were washed once in PBS. The click chemistry reaction was composed of Tris(2-carboxyethyl)phosphine (TCEP) (Thermo), Tris[(1-benzyl-1H-1,2,3-triazol-4-yl)methyl]amine (TBTA) (Sigma). The reaction was allowed to proceed for 1 hour. Cover slips were washed in 0.1% TritonX in PBS 3 time, 15 minutes each and mounted microscopy slides using DAPI-containing mounting solution.

Image acquisition and analysis

Slides were imaged using a custom epifluorescence microscope equipped with a Plan-Apochromatic 40X (NA 1.4) objective (Zeiss), illuminated with a LED light source (Model Spectra-6LCR-SA, Lumencor) and the emitted fluorescence collected with a CMOS camera (Hamamatsu ORCA-Flash 4.0). The microscope was controlled using µManager (Edelstein et al., 2014). A custom pipeline was employed to compute total fluorescence intensity per cell using Cellprofiler (Broad Institute) (Carpenter et al., 2006).

Western Blotting

Cells were lysed in 1x RIPA buffer, boiled in SDS and run on SDS-PAGE. Proteins were transferred onto nitrocellulose membrane, blocked in 5% milk and probed with the following antibodies: NPM1 (Abcam, 1:1000), IPO7 (Abcam, 1:1000), TP53 (Bethyl, 1:500), Cyclin A2 (BD Biosciences, 1:1000), Tubulin (Abcam, 1:1000), Actin (Sigma, 1:10000).

Viability assay

To assess changes in cell viability, cells were counted using an automated cell counter (BioRad) and equal number of cells were plated in a 96 well plate. On the sixth day of the siRNA experiment, fresh medium was added that contained 1:10 dilution of the WST1 reagent (Sigma). Cells were incubated for different time points before the absorbance was measured at 450 nm using a plate reader (BioRad).

Apoptosis assay

Apoptotic induction was examined by checking for Active Caspase-3 levels using a PE-conjugated anti-Caspase-3 antibody per the manufacturer's instructions (BD Biosciences). PE levels were examined using an LSRII flow cytometer (BD Biosciences).

Cell cycle analysis

Cell cycle progression was examined using the Click-it Alexa Fluor 647 kit (Thermo). Briefly, cells were plated on cover slips. After 24 hours, cells were pulsed in Edu for 10 minutes and then fixed in 4%

paraformaldehyde in PBS, permeabilized in 0.1% TritonX in PBS. Cells were then washed twice in 2% BSA in PBS. The EdU was reacted with azide-conjugated fluorophore in the presence of Copper sulfate. The click chemistry reaction was allowed to proceed for 1 hour. Cells were washed twice in 2% BSA in PBS. DNA was labelled using Hoechst at a dilution of 1:10000 mounted on Prolong Gold mounting solution (Thermo). The fraction of cells in each stage of the cell cycle was quantified using a custom Matlab script (Mathworks).

Northern blotting

Equal numbers of cells were harvested for all conditions using the Luna Automated Cell Counter (Logos Biosystems). Total RNA was extracted using Trizol (Thermo) according to the manufacturer's instructions. The RNA was separated on a denaturing gel and transferred to nylon membrane (GE healthcare) overnight as previously described (Akef et al., 2015). The membrane was hybridized to a ^{32}P-labeled probe overnight and imaged using a Typhoon phosphoimager (Molecular Dynamics). To probe for the ITS2, an oligonucleotide was 5'-labeled using PNK enzyme (NEB). The ITS2 probe was previously reported (Donati et al., 2013) and its sequence is GAGGGAGGAACCCGGACCGCAGGCGGCGGCCACGGGAACTCGGCCCGAGCCGGCTCTCTC. For GAPDH probe, the pET30-2-GAPDH plasmids was a gift from David Sabatini (Addgene plasmid # 83910) (Pacold et al., 2016) and gene-body labeling was performed using the Prime-A-Gene kit (Promega).

Mutual Exclusivity of U2AF1 and NPM1 mutations

Cancer patient data was retrieved from cBioPortal (www.cbioportal.org) as of October, 4th, 2019. All adult AML and MDS patient studies were selected. These include: "Acute myeloid leukemia or myelodysplastic syndromes (Wash U, 2016)", "Acute myeloid leukemia (OHSU, 2018)", "Acute myeloid leukemia (TCGA, PanCancer Atlas)", and "Myelodysplasia (UTokyo, Nature 2011)".

Online supplemental material:

Fig. S1 shows gating strategies used from representative apoptosis and cell cycle experiments.

Acknowledgements:

This work was supported by the intramural research program of the National Cancer Institute. We thank Dr. Jeff Coller for sharing rRNA northern blotting protocols. We also thank members of the Larson lab for comments on the manuscript. The authors declare no competing financial interests.

Author contributions:

Abdalla Akef and Daniel R. Larson conceived and designed the study. Abdalla Akef performed most experiments and analyzed data. Daniel R. Larson analyzed the polysome profiling data. Steven D. Cappell contributed software for cell cycle analysis. Abdalla Akef and Daniel R. Larson wrote the manuscript with feedback from Steven D. Cappell.

References

Abelson, S., G. Collord, S.W.K. Ng, O. Weissbrod, N.M. Cohen, E. Niemeyer, N. Barda, P.C. Zuzarte, L. Heisler, Y. Sundaravadanam, R. Luben, S. Hayat, T.T. Wang, Z. Zhao, I. Cirlan, T.J. Pugh, D. Soave, K. Ng, C. Latimer, C. Hardy, K. Raine, D. Jones, D. Hoult, A. Britten, J.D. McPherson, M. Johansson, F. Mbabaali, J. Eagles, J.K. Miller, D. Pasternack, L. Timms, P. Krzyzanowski, P. Awadalla, R. Costa, E. Segal, S.V. Bratman, P. Beer, S. Behjati, I. Martincorena, J.C.Y. Wang, K.M. Bowles, J.R. Quirós, A. Karakatsani, C.L. Vecchia, A. Trichopoulou, E. Salamanca-Fernández, J.M. Huerta, A. Barricarte, R.C. Travis, R. Tumino, G. Masala, H. Boeing, S. Panico, R. Kaaks, A. Krämer, S. Sieri, E. Riboli, P. Vineis, M. Foll, J. McKay, S. Polidoro, N. Sala, K.-T. Khaw, R. Vermeulen, P.J. Campbell, E. Papaemmanuil, M.D. Minden, A. Tanay, R.D. Balicer, N.J. Wareham, M. Gerstung, J.E. Dick, P. Brennan, G.S. Vassiliou, and L.I. Shlush. 2018. Prediction of acute myeloid leukaemia risk in healthy individuals. *Nature*. 559:400–404. doi:10.1038/s41586-018-0317-6.

Akef, A., E.S. Lee, and A.F. Palazzo. 2015. Splicing promotes the nuclear export of β-globin mRNA by overcoming nuclear retention elements. *RNA N. Y. N.* 21:1908–1920. doi:10.1261/rna.051987.115.

Bertwistle, D., M. Sugimoto, and C.J. Sherr. 2004. Physical and functional interactions of the Arf tumor suppressor protein with nucleophosmin/B23. *Mol. Cell. Biol.* 24:985–996.

den Besten, W., M.-L. Kuo, R.T. Williams, and C.J. Sherr. 2005. Myeloid leukemia-associated nucleophosmin mutants perturb p53-dependent and independent activities of the Arf tumor suppressor protein. *Cell Cycle Georget. Tex*. 4:1593–1598. doi:10.4161/cc.4.11.2174.

Brooks, A.N., P.S. Choi, L. de Waal, T. Sharifnia, M. Imielinski, G. Saksena, C.S. Pedamallu, A. Sivachenko, M. Rosenberg, J. Chmielecki, M.S. Lawrence, D.S. DeLuca, G. Getz, and M. Meyerson. 2014. A pan-cancer analysis of transcriptome changes associated with somatic mutations in U2AF1 reveals commonly altered splicing events. *PloS One*. 9:e87361. doi:10.1371/journal.pone.0087361.

Brunetti, L., M.C. Gundry, D. Sorcini, A.G. Guzman, Y.-H. Huang, R. Ramabadran, I. Gionfriddo, F. Mezzasoma, F. Milano, B. Nabet, D.L. Buckley, S.M. Kornblau, C.Y. Lin, P. Sportoletti, M.P. Martelli, B. Falini, and M.A. Goodell. 2018. Mutant NPM1 Maintains the Leukemic State through HOX Expression. *Cancer Cell*. 34:499-512.e9. doi:10.1016/j.ccell.2018.08.005.

Carpenter, A.E., T.R. Jones, M.R. Lamprecht, C. Clarke, I.H. Kang, O. Friman, D.A. Guertin, J.H. Chang, R.A. Lindquist, J. Moffat, P. Golland, and D.M. Sabatini. 2006. CellProfiler: image analysis software for identifying and quantifying cell phenotypes. *Genome Biol.* 7:R100. doi:10.1186/gb-2006-7-10-r100.

Castle, C.D., E.K. Cassimere, and C. Denicourt. 2012. LAS1L interacts with the mammalian Rix1 complex to regulate ribosome biogenesis. *Mol. Biol. Cell*. 23:716–728. doi:10.1091/mbc.E11-06-0530.

Coller, J., and R. Parker. 2005. General translational repression by activators of mRNA decapping. *Cell*. 122:875–886. doi:10.1016/j.cell.2005.07.012.

Colombo, E., J.-C. Marine, D. Danovi, B. Falini, and P.G. Pelicci. 2002. Nucleophosmin regulates the stability and transcriptional activity of p53. *Nat. Cell Biol.* 4:529–533. doi:10.1038/ncb814.

Donati, G., S. Peddigari, C.A. Mercer, and G. Thomas. 2013. 5S ribosomal RNA is an essential component of a nascent ribosomal precursor complex that regulates the Hdm2-p53 checkpoint. *Cell Rep.* 4:87–98. doi:10.1016/j.celrep.2013.05.045.

Edelstein, A.D., M.A. Tsuchida, N. Amodaj, H. Pinkard, R.D. Vale, and N. Stuurman. 2014. Advanced methods of microscope control using μManager software. *J. Biol. Methods*. 1. doi:10.14440/jbm.2014.36.

Falini, B., C. Mecucci, E. Tiacci, M. Alcalay, R. Rosati, L. Pasqualucci, R. La Starza, D. Diverio, E. Colombo, A. Santucci, B. Bigerna, R. Pacini, A. Pucciarini, A. Liso, M. Vignetti, P. Fazi, N. Meani, V. Pettirossi, G. Saglio, F. Mandelli, F. Lo-Coco, P.-G. Pelicci, M.F. Martelli, and GIMEMA Acute Leukemia Working Party. 2005. Cytoplasmic nucleophosmin in acute myelogenous leukemia with a normal karyotype. *N. Engl. J. Med.* 352:254–266. doi:10.1056/NEJMoa041974.

Fei, D.L., H. Motowski, R. Chatrikhi, S. Prasad, J. Yu, S. Gao, C.L. Kielkopf, R.K. Bradley, and H. Varmus. 2016. Wild-Type U2AF1 Antagonizes the Splicing Program Characteristic of U2AF1-Mutant Tumors and Is Required for Cell Survival. *PLoS Genet.* 12:e1006384. doi:10.1371/journal.pgen.1006384.

Fernández, I.S., X.-C. Bai, G. Murshudov, S.H.W. Scheres, and V. Ramakrishnan. 2014. Initiation of Translation by Cricket Paralysis Virus IRES Requires Its Translocation in the Ribosome. *Cell*. 157:823–831. doi:10.1016/j.cell.2014.04.015.

Gillery, P., N. Georges, J. Wegrowski, A. Randoux, and J.P. Borel. 1995. Protein synthesis in collagen lattice-cultured fibroblasts is controlled at the ribosomal level. *FEBS Lett.* 357:287–289. doi:10.1016/0014-5793(94)01375-b.

Golomb, L., D.R. Bublik, S. Wilder, R. Nevo, V. Kiss, K. Grabusic, S. Volarevic, and M. Oren. 2012. Importin 7 and exportin 1 link c-Myc and p53 to regulation of ribosomal biogenesis. *Mol. Cell*. 45:222–232. doi:10.1016/j.molcel.2011.11.022.

Grisendi, S., R. Bernardi, M. Rossi, K. Cheng, L. Khandker, K. Manova, and P.P. Pandolfi. 2005. Role of nucleophosmin in embryonic development and tumorigenesis. *Nature*. 437:147–153. doi:10.1038/nature03915.

Halle, J.P., S. Müller, A. Simm, and G. Adam. 1997. Copy number, epigenetic state and expression of the rRNA genes in young and senescent rat embryo fibroblasts. *Eur. J. Cell Biol.* 74:281–288.

Herrera, J.E., R. Savkur, and M.O. Olson. 1995. The ribonuclease activity of nucleolar protein B23. *Nucleic Acids Res.* 23:3974–3979.

Huang, N., S. Negi, A. Szebeni, and M.O.J. Olson. 2005. Protein NPM3 interacts with the multifunctional nucleolar protein B23/nucleophosmin and inhibits ribosome biogenesis. *J. Biol. Chem.* 280:5496–5502. doi:10.1074/jbc.M407856200.

Itahana, K., K.P. Bhat, A. Jin, Y. Itahana, D. Hawke, R. Kobayashi, and Y. Zhang. 2003. Tumor suppressor ARF degrades B23, a nucleolar protein involved in ribosome biogenesis and cell proliferation. *Mol. Cell*. 12:1151–1164.

Khajuria, R.K., M. Munschauer, J.C. Ulirsch, C. Fiorini, L.S. Ludwig, S.K. McFarland, N.J. Abdulhay, H. Specht, H. Keshishian, D.R. Mani, M. Jovanovic, S.R. Ellis, C.P. Fulco, J.M. Engreitz, S. Schütz, J. Lian, K.W. Gripp, O.K. Weinberg, G.S. Pinkus, L. Gehrke, A. Regev, E.S. Lander, H.T. Gazda, W.Y. Lee, V.G. Panse, S.A. Carr, and V.G. Sankaran. 2018. Ribosome Levels Selectively Regulate Translation and Lineage Commitment in Human Hematopoiesis. *Cell*. 173:90-103.e19. doi:10.1016/j.cell.2018.02.036.

Korgaonkar, C., J. Hagen, V. Tompkins, A.A. Frazier, C. Allamargot, F.W. Quelle, and D.E. Quelle. 2005. Nucleophosmin (B23) targets ARF to nucleoli and inhibits its function. *Mol. Cell. Biol.* 25:1258–1271. doi:10.1128/MCB.25.4.1258-1271.2005.

Maggi, L.B., M. Kuchenruether, D.Y.A. Dadey, R.M. Schwope, S. Grisendi, R.R. Townsend, P.P. Pandolfi, and J.D. Weber. 2008. Nucleophosmin serves as a rate-limiting nuclear export chaperone for the Mammalian ribosome. *Mol. Cell. Biol.* 28:7050–7065. doi:10.1128/MCB.01548-07.

Mariano, A.R., E. Colombo, L. Luzi, P. Martinelli, S. Volorio, L. Bernard, N. Meani, R. Bergomas, M. Alcalay, and P.G. Pelicci. 2006. Cytoplasmic localization of NPM in myeloid leukemias is dictated by gain-of-function mutations that create a functional nuclear export signal. *Oncogene*. 25:4376–4380. doi:10.1038/sj.onc.1209453.

Marks, M.S. 2001. Determination of molecular size by zonal sedimentation analysis on sucrose density gradients. *Curr. Protoc. Cell Biol.* Chapter 5:Unit 5.3. doi:10.1002/0471143030.cb0503s00.

Merendino, L., S. Guth, D. Bilbao, C. Martínez, and J. Valcárcel. 1999. Inhibition of msl-2 splicing by Sex-lethal reveals interaction between U2AF35 and the 3' splice site AG. *Nature*. 402:838–841. doi:10.1038/45602.

Metsalu, T., and J. Vilo. 2015. ClustVis: a web tool for visualizing clustering of multivariate data using Principal Component Analysis and heatmap. *Nucleic Acids Res.* 43:W566-570. doi:10.1093/nar/gkv468.

Okuda, M., H.F. Horn, P. Tarapore, Y. Tokuyama, A.G. Smulian, P.K. Chan, E.S. Knudsen, I.A. Hofmann, J.D. Snyder, K.E. Bove, and K. Fukasawa. 2000. Nucleophosmin/B23 is a target of CDK2/cyclin E in centrosome duplication. *Cell*. 103:127–140.

Pacold, M.E., K.R. Brimacombe, S.H. Chan, J.M. Rohde, C.A. Lewis, L.J.Y.M. Swier, R. Possemato, W.W. Chen, L.B. Sullivan, B.P. Fiske, S. Cho, E. Freinkman, K. Birsoy, M. Abu-Remaileh, Y.D. Shaul, C.M. Liu, M. Zhou, M.J. Koh, H. Chung, S.M. Davidson, A. Luengo, A.Q. Wang, X. Xu, A. Yasgar, L. Liu, G. Rai, K.D. Westover, M.G. Vander Heiden, M. Shen, N.S. Gray, M.B. Boxer, and D.M. Sabatini. 2016. A PHGDH inhibitor reveals coordination of serine synthesis and one-carbon unit fate. *Nat. Chem. Biol.* 12:452–458. doi:10.1038/nchembio.2070.

Palangat, M., D.G. Anastasakis, D.L. Fei, K.E. Lindblad, R. Bradley, C.S. Hourigan, M. Hafner, and D.R. Larson. 2019. The splicing factor U2AF1 contributes to cancer progression through a noncanonical role in translation regulation. *Genes Dev.* doi:10.1101/gad.319590.118.

Pelletier, C.L., L.B. Maggi, S.N. Brady, D.K. Scheidenhelm, D.H. Gutmann, and J.D. Weber. 2007. TSC1 sets the rate of ribosome export and protein synthesis through nucleophosmin translation. *Cancer Res.* 67:1609–1617. doi:10.1158/0008-5472.CAN-06-2875.

Ramirez, R.D., S. Sheridan, L. Girard, M. Sato, Y. Kim, J. Pollack, M. Peyton, Y. Zou, J.M. Kurie, J.M. Dimaio, S. Milchgrub, A.L. Smith, R.F. Souza, L. Gilbey, X. Zhang, K. Gandia, M.B. Vaughan, W.E. Wright, A.F. Gazdar, J.W. Shay, and J.D. Minna. 2004. Immortalization of human bronchial epithelial cells in the absence of viral oncoproteins. *Cancer Res.* 64:9027–9034. doi:10.1158/0008-5472.CAN-04-3703.

Salic, A., and T.J. Mitchison. 2008. A chemical method for fast and sensitive detection of DNA synthesis in vivo. *Proc. Natl. Acad. Sci. U. S. A.* 105:2415–2420. doi:10.1073/pnas.0712168105.

Savkur, R.S., and M.O. Olson. 1998. Preferential cleavage in pre-ribosomal RNA byprotein B23 endoribonuclease. *Nucleic Acids Res.* 26:4508–4515.

Stevens, B.M., N. Khan, A. D'Alessandro, T. Nemkov, A. Winters, C.L. Jones, W. Zhang, D.A. Pollyea, and C.T. Jordan. 2018. Characterization and targeting of malignant stem cells in patients with advanced myelodysplastic syndromes. *Nat. Commun.* 9:3694. doi:10.1038/s41467-018-05984-x.

Tom Dieck, S., A. Müller, A. Nehring, F.I. Hinz, I. Bartnik, E.M. Schuman, and D.C. Dieterich. 2012. Metabolic labeling with noncanonical amino acids and visualization by chemoselective fluorescent tagging. *Curr. Protoc. Cell Biol.* Chapter 7:Unit7.11. doi:10.1002/0471143030.cb0711s56.

Tovar, C., J. Rosinski, Z. Filipovic, B. Higgins, K. Kolinsky, H. Hilton, X. Zhao, B.T. Vu, W. Qing, K. Packman, O. Myklebost, D.C. Heimbrook, and L.T. Vassilev. 2006. Small-molecule MDM2 antagonists reveal aberrant p53 signaling in cancer: implications for therapy. *Proc. Natl. Acad. Sci. U. S. A.* 103:1888–1893. doi:10.1073/pnas.0507493103.

Volarevic, S., M.J. Stewart, B. Ledermann, F. Zilberman, L. Terracciano, E. Montini, M. Grompe, S.C. Kozma, and G. Thomas. 2000. Proliferation, but not growth, blocked by conditional deletion of 40S ribosomal protein S6. *Science*. 288:2045–2047.

Yoshida, K., M. Sanada, Y. Shiraishi, D. Nowak, Y. Nagata, R. Yamamoto, Y. Sato, A. Sato-Otsubo, A. Kon, M. Nagasaki, G. Chalkidis, Y. Suzuki, M. Shiosaka, R. Kawahata, T. Yamaguchi, M. Otsu, N. Obara, M. Sakata-Yanagimoto, K. Ishiyama, H. Mori, F. Nolte, W.-K. Hofmann, S. Miyawaki, S. Sugano, C. Haferlach, H.P. Koeffler, L.-Y. Shih, T. Haferlach, S. Chiba, H. Nakauchi, S. Miyano, and S. Ogawa. 2011. Frequent pathway mutations of splicing machinery in myelodysplasia. *Nature*. 478:64–69. doi:10.1038/nature10496.

Yoshimi, A., K.-T. Lin, D.H. Wiseman, M.A. Rahman, A. Pastore, B. Wang, S.C.-W. Lee, J.-B. Micol, X.J. Zhang, S. de Botton, V. Penard-Lacronique, E.M. Stein, H. Cho, R.E. Miles, D. Inoue, T.R. Albrecht, T.C.P. Somervaille, K. Batta, F. Amaral, F. Simeoni, D.P. Wilks, C. Cargo, A.M. Intlekofer, R.L. Levine, H. Dvinge, R.K. Bradley, E.J. Wagner, A.R. Krainer, and O. Abdel-Wahab. 2019. Coordinated alterations in RNA splicing and epigenetic regulation drive leukaemogenesis. *Nature*. doi:10.1038/s41586-019-1618-0.

Abbreviations:

AML: Acute Myeloid Leukemia

EdU: 5-ethynyl-2’-deoxyuridine

IPO7: Importin 7

MDS: Myelodysplastic Syndrome

NPM1: Nucleophosmin 1

U2AF1: U2 Small Nuclear RNA Auxiliary Factor 1

Figure Legends

Figure 1. The U2AF1-S34F mutation upregulates a subset of translation and ribosome biogenesis factors and increases nascent polypeptide production.

(A) Heat map of mRNA enrichment in the polysome fraction of translation and ribosome biogenesis factors in wt/wt, wt/S34F, wt/S34F- cells. (B) A schematic diagram of the *NPM1-luciferase* reporter. The reporter consists of NPM1 exon 1, Renilla luciferase, CrPV IRES, Firefly luciferase. (C) Normalized Renilla to Firefly luciferase activity demonstrates elevated translation levels of the *NPM1-luciferase* reporter. * = $p < 0.05$. (D) Puromycin treatment abrogates the nascent polypeptide fluorescence signal. Scale bar = 10 µm. (E-G) The U2AF1-S34F mutation upregulates global nascent polypeptide production. The cells were imaged (E) and total cellular fluorescence intensity was quantified (F). Each bar represents the average and standard error of four independent experiments. * = $p < 0.05$. Scale bar = 10 µm. (G) Cumulative Fluorescence intensity of the AHA signal.

Figure 2. NPM1 and IPO7 are required for the viability of the wt/S34F cells.

(A) Cells treated with siRNA directed against NPM1 were lysed and proteins separated on SDS-PAGE and analyzed by immunoblot using antibodies against NPM1 and α-Tubulin. (B) Cells treated with the indicated siRNAs were imaged 144 hours post-siRNA transfection. Scale bar = 50 µm. (C) Quantification of cell viability using the WST1 reagent. Each bar represents the average and standard error of three independent experiments. * = $p < 0.05$ using a paired 2-sided t-test. (D) Cells treated with siRNA directed against IPO7 were lysed and proteins separated on SDS-PAGE and analyzed by immunoblot using antibodies against IPO7 and β-Actin. (E) Quantification of cell viability using the WST1 reagent. Each bar represents the average and standard error of three independent experiments. * = $p < 0.05$ using a paired 2-sided t-test. (F) Cells that express either $NPM1^r$-2A-GFP or empty vector were treated with siRNA directed against NPM1 were lysed and proteins separated on SDS-PAGE and analyzed by immunoblot using antibodies against NPM1 and β-Actin. (G) Quantification of cell viability using the WST1 reagent. Each bar represents the average and standard error of three independent experiments. * = $p < 0.05$ using a paired 2-sided t-test.

Figure 3. The requirement of wt/S34F cells for NPM1 is independent of TP53.

(A) Cells treated with siRNA directed against NPM1 were lysed and proteins separated on SDS-PAGE and analyzed by immunoblot using antibodies against NPM1 and α-Tubulin. (B) Cells treated with the indicated siRNAs were imaged 144 hours post-siRNA transfection. Scale bar = 50 µm. (C) Quantification of cell viability using the WST1 reagent. Each bar represents the average and standard error of three independent experiments. * = $p < 0.05$ using a paired 2-sided t-test. (D) Cells treated with 10µM Nutlin3A for 36 hours were lysed and proteins separated on SDS-PAGE and analyzed by immunoblot using antibodies against NPM1, p53 and β-Actin. (E) Nutlin3A treatment impairs the viability of wt/wt, wt/S34F and wt/S34F- cells. Scale bar = 50 µm. (F) Cell viability was assessed 36 hours after treatment with the indicated doses of Nutlin3A using the WST1 reagent.

Figure 4. NPM1 or IPO7 silencing slows the proliferation of S34F cells.

(A) The viability of cells treated with siRNAs directed against NPM1 or IPO7 was assessed at the indicated timepoints post-siRNA transfection. Error bars represent the standard error of three independent experiments. (B) Quantification of the active Caspase-3 levels. Each bar represents the average and standard error of three independent experiments. (C) Cells that express either $NPM1^{r}$-2A-GFP or empty vector were treated with siRNA directed against NPM1. 144 hours post-siRNA transfection, cells were pulsed with EdU for 10 minutes and EdU incorporation was quantified. The fraction of cells in each phase of the cell cycle was calculated. Each bar represents the average and standard error of three independent experiments. * = $p < 0.05$ using a paired 2-sided t-test. (D) Cells were treated with siRNA directed against IPO7. 144 hours post-siRNA transfection, cells were pulsed with EdU for 10 minutes and EdU incorporation was quantified. The fraction of cells in each phase of the cell cycle was calculated. Each bar represents the average and standard error of three independent experiments. * = $p < 0.05$ using a paired 2-sided t-test. (E-F) Cells treated with siRNA directed against NPM1 (E) or IPO7 (F) were lysed and

proteins separated on SDS-PAGE and analyzed by immunoblot using antibodies against Cyclin A2, NPM1 or IPO7 and β-Actin.

Figure 5. Silencing NPM1 or IPO7 impairs rRNA precursor levels in wt/S34F cells.

(A and B) The levels of the ITS2-containing rRNA precursors are decreased in wt/S34F cells depleted of NPM1 (A) or IPO7 (B). (C) U2AF1 and NPM1 mutations are mutually exclusive in MDS and AML patients (q value < 0.001).

Supplementary Figure Legends

Figure S1. Gating Strategy from representative Caspase-3 and EdU labeling experiments.

Figure 1:

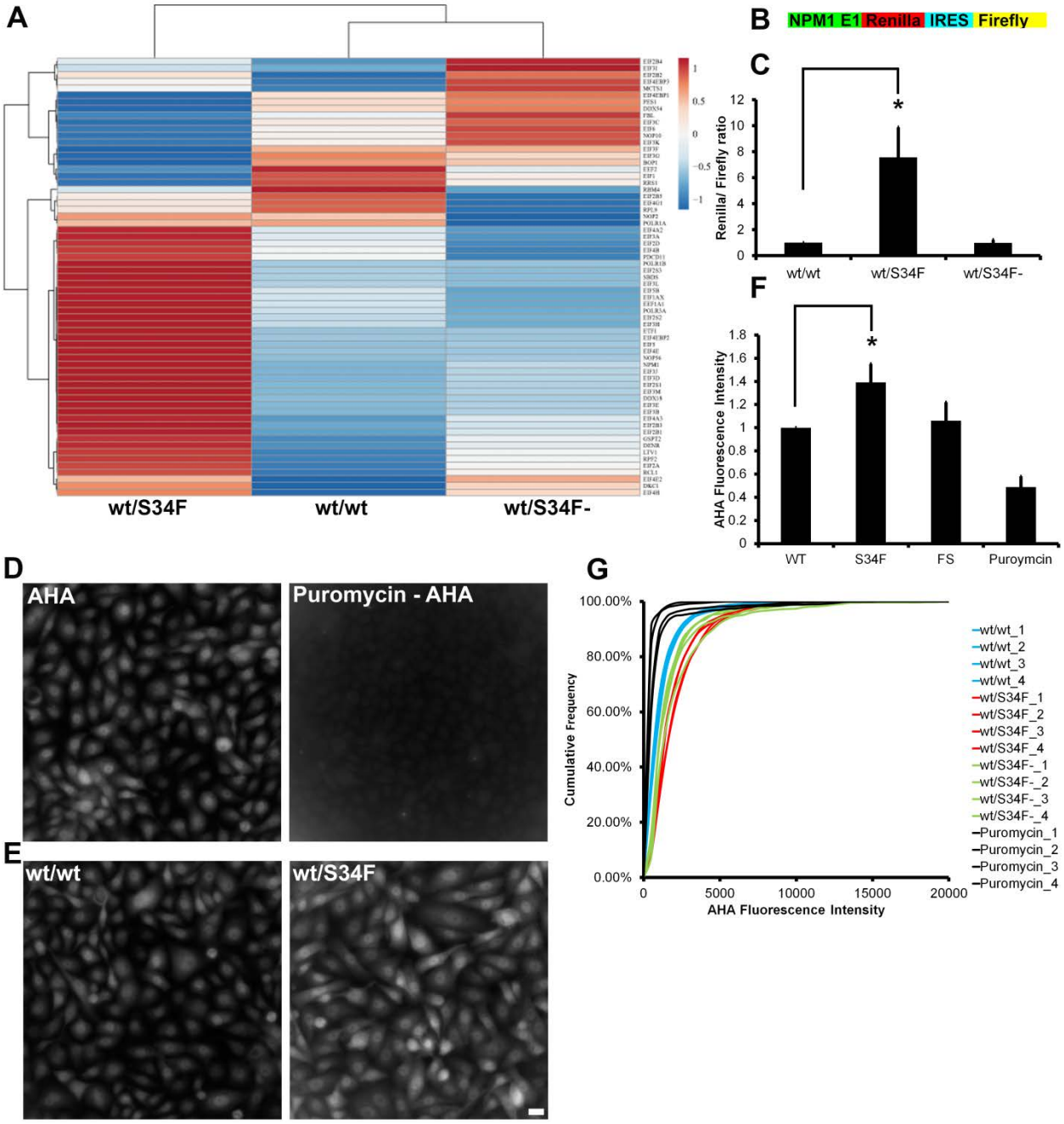
A
wt/S34F
wt/wt
wt/S34F-
B
NPM1 E1 Renilla IRES Firefly
C
Renilla/ Firefly ratio
wt/wt
wt/S34F
wt/S34F-
F
AHA Fluorescence Intensity
WT
S34F
FS
Puroymcin
D
AHA
Puromycin - AHA
E
wt/wt
wt/S34F
G
Cumulative Frequency
AHA Fluorescence Intensity
wt/wt_1
wt/wt_2
wt/wt_3
wt/wt_4
wt/S34F_1
wt/S34F_2
wt/S34F_3
wt/S34F_4
wt/S34F-_1
wt/S34F-_2
wt/S34F-_3
wt/S34F-_4
Puromycin_1
Puromycin_2
Puromycin_3
Puromycin_4

Figure 2:

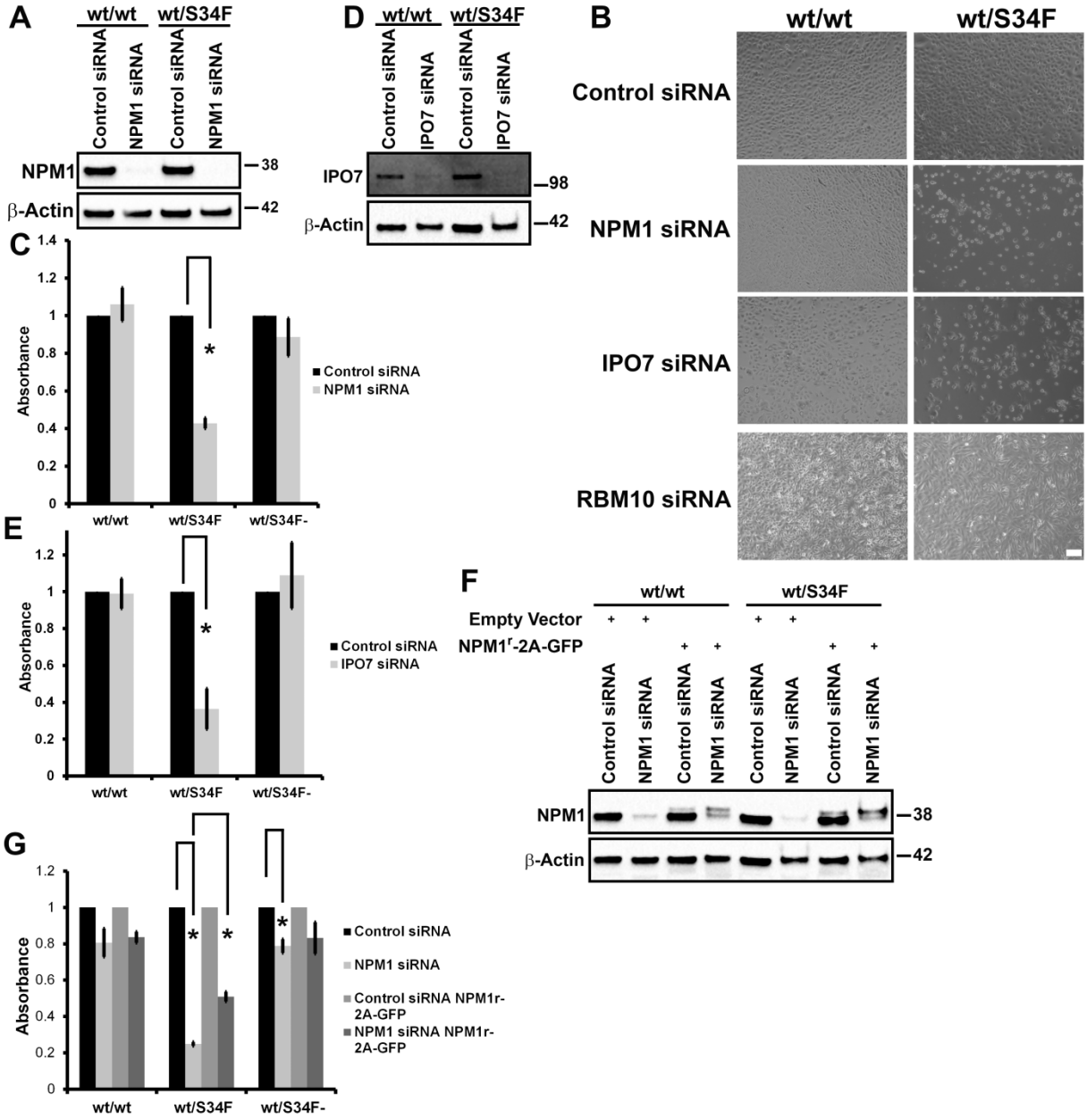
A
wt/wt
wt/S34F
Control siRNA
NPM1 siRNA
Control siRNA
NPM1 siRNA
NPM1
β-Actin
38
42
D
wt/wt
wt/S34F
Control siRNA
IPO7 siRNA
Control siRNA
IPO7 siRNA
IPO7
β-Actin
98
42
B
wt/wt
wt/S34F
Control siRNA
NPM1 siRNA
IPO7 siRNA
RBM10 siRNA
C
Absorbance
Control siRNA
NPM1 siRNA
wt/wt
wt/S34F
wt/S34F-
E
Absorbance
Control siRNA
IPO7 siRNA
wt/wt
wt/S34F
wt/S34F-
F
wt/wt
wt/S34F
Empty Vector
NPM1r-2A-GFP
Control siRNA
NPM1 siRNA
Control siRNA
NPM1 siRNA
Control siRNA
NPM1 siRNA
Control siRNA
NPM1 siRNA
NPM1
β-Actin
38
42
G
Absorbance
Control siRNA
NPM1 siRNA
Control siRNA NPM1r-2A-GFP
NPM1 siRNA NPM1r-2A-GFP
wt/wt
wt/S34F
wt/S34F-

Figure 3:

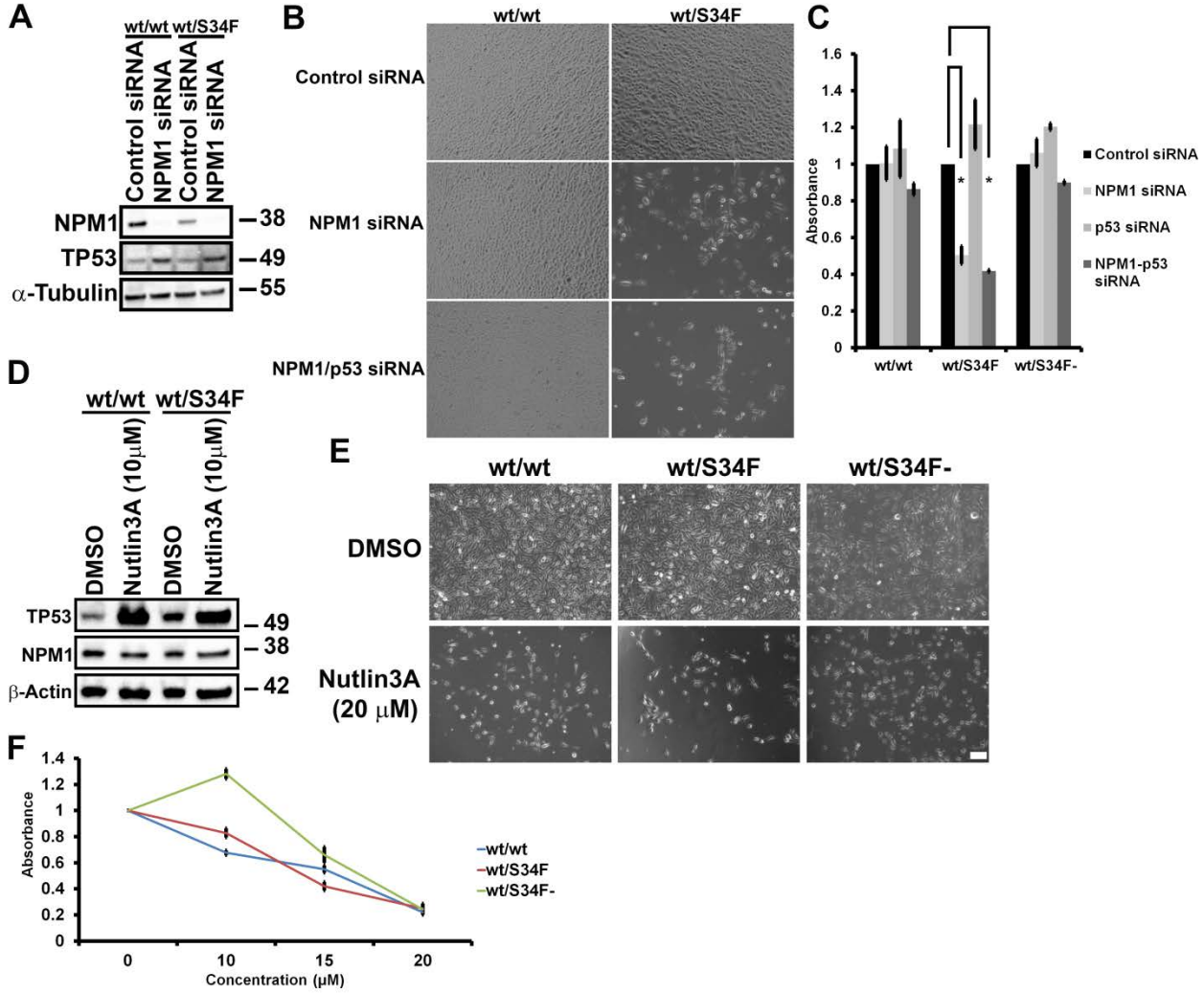
A
wt/wt wt/S34F
Control siRNA
NPM1 siRNA
Control siRNA
NPM1 siRNA
NPM1
TP53
α-Tubulin
38
49
55
B
wt/wt
wt/S34F
Control siRNA
NPM1 siRNA
NPM1/p53 siRNA
C
Absorbance
Control siRNA
NPM1 siRNA
p53 siRNA
NPM1-p53 siRNA
wt/wt
wt/S34F
wt/S34F-
D
wt/wt wt/S34F
DMSO
Nutlin3A (10μM)
DMSO
Nutlin3A (10μM)
TP53
NPM1
β-Actin
49
38
42
E
wt/wt
wt/S34F
wt/S34F-
DMSO
Nutlin3A (20 μM)
F
Absorbance
Concentration (μM)
wt/wt
wt/S34F
wt/S34F-

Figure 4:

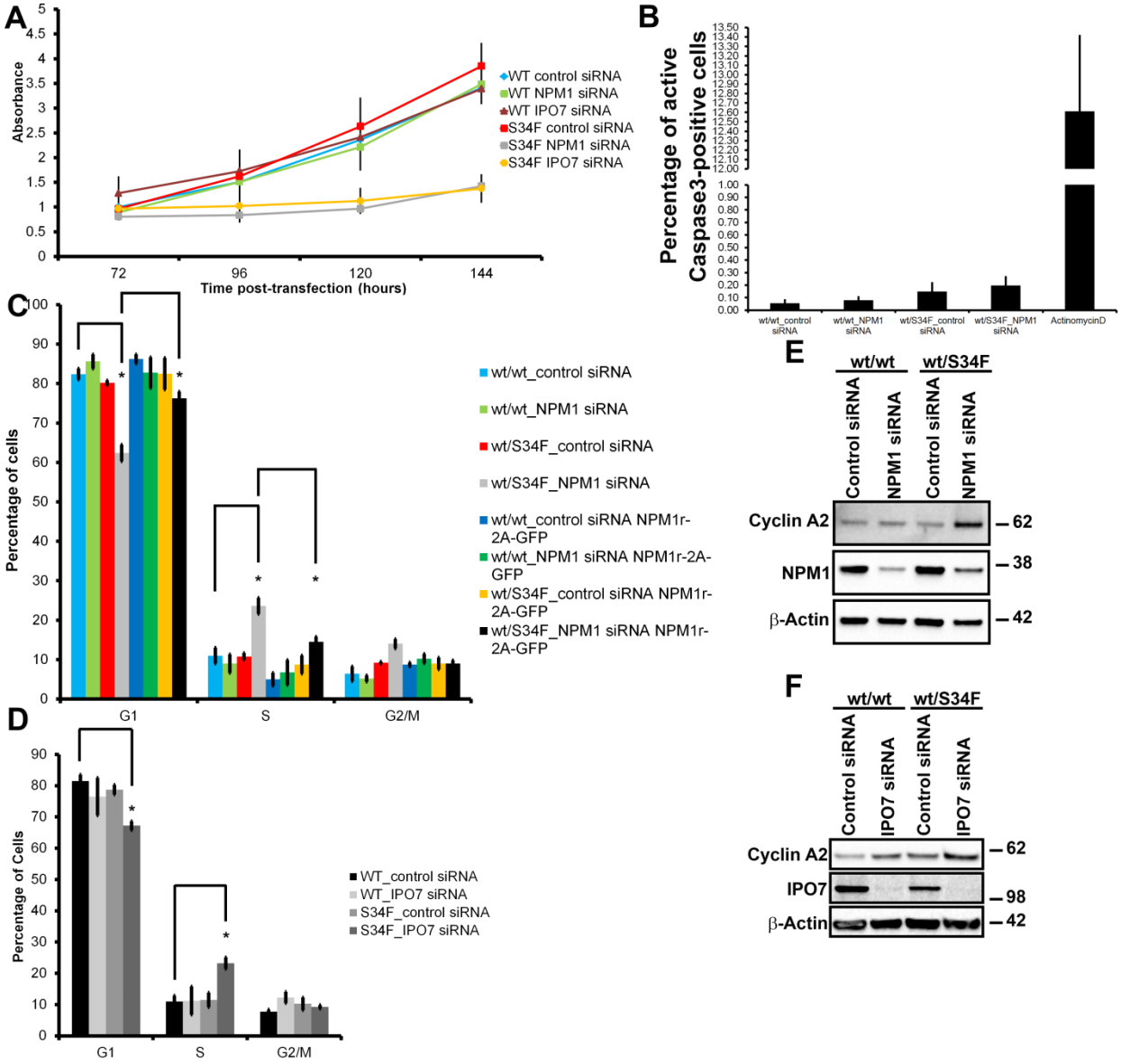
A
Absorbance
Time post-transfection (hours)
WT control siRNA
WT NPM1 siRNA
WT IPO7 siRNA
S34F control siRNA
S34F NPM1 siRNA
S34F IPO7 siRNA
B
Percentage of active Caspase3-positive cells
wt/wt_control siRNA
wt/wt_NPM1 siRNA
wt/S34F_control siRNA
wt/S34F_NPM1 siRNA
ActinomycinD
C
Percentage of cells
wt/wt_control siRNA
wt/wt_NPM1 siRNA
wt/S34F_control siRNA
wt/S34F_NPM1 siRNA
wt/wt_control siRNA NPM1r-2A-GFP
wt/wt_NPM1 siRNA NPM1r-2A-GFP
wt/S34F_control siRNA NPM1r-2A-GFP
wt/S34F_NPM1 siRNA NPM1r-2A-GFP
G1
S
G2/M
D
Percentage of Cells
WT_control siRNA
WT_IPO7 siRNA
S34F_control siRNA
S34F_IPO7 siRNA
G1
S
G2/M
E
wt/wt
wt/S34F
Control siRNA
NPM1 siRNA
Control siRNA
NPM1 siRNA
Cyclin A2
NPM1
β-Actin
62
38
42
F
wt/wt
wt/S34F
Control siRNA
IPO7 siRNA
Control siRNA
IPO7 siRNA
Cyclin A2
IPO7
β-Actin
62
98
42

Figure 5:

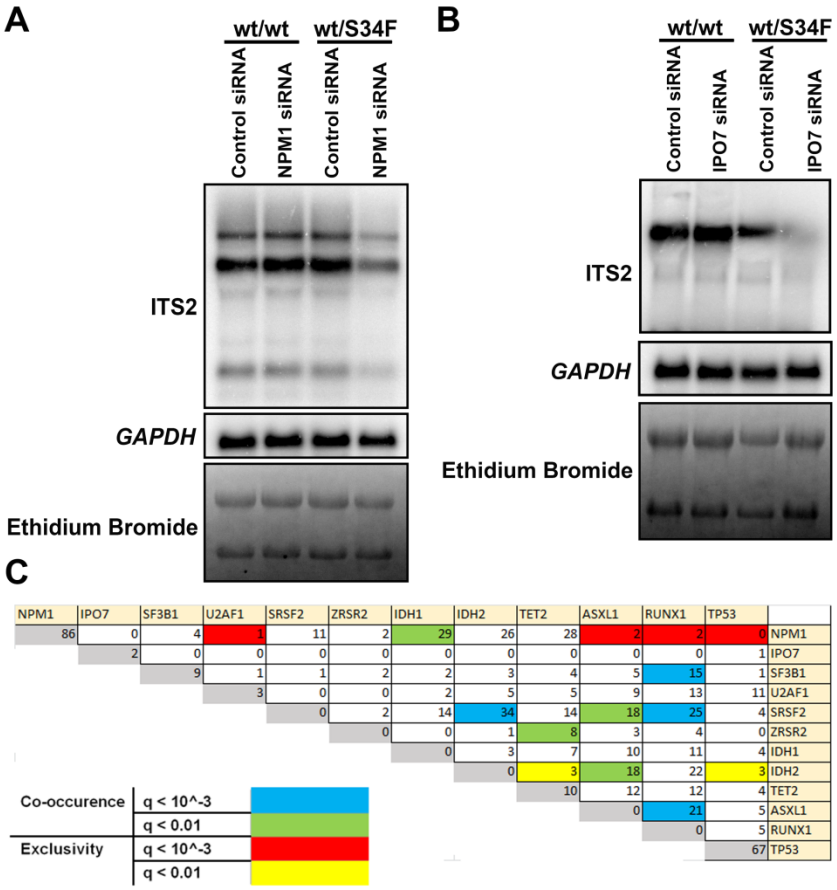

	NPM1	IPO7	SF3B1	U2AF1	SRSF2	ZRSR2	IDH1	IDH2	TET2	ASXL1	RUNX1	TP53
NPM1	86	0	4	1	11	2	29	26	28	2	2	0
IPO7		2	0	0	0	0	0	0	0	0	0	1
SF3B1			9	1	1	2	2	3	4	5	15	1
U2AF1				3	0	0	2	5	5	9	13	11
SRSF2					0	2	14	34	14	18	25	4
ZRSR2						0	0	1	8	3	4	0
IDH1							0	3	7	10	11	4
IDH2								0	3	18	22	3
TET2									10	12	12	4
ASXL1										0	21	5
RUNX1											0	5
TP53												67